The unusual stratospheric Arctic winter 2019/20: Chemical ozone loss from satellite observations and TOMCAT chemical transport model

Mark Weber[1], Carlo Arosio[1], Wuhu Feng[2], Sandip Dhomse[2], Martyn P. Chipperfield[2], Andreas Meier[1], John P Burrows[1], Kai-Uwe Eichmann[1], Andreas Richter[1], and Alexei Rozanov[1]

[1]University of Bremen FB1
[2]University of Leeds

November 26, 2022

Abstract

Satellite observations of relevant trace gases, together with meteorological data from ERA5, were used to describe the dynamics and chemistry of the spectacular Arctic 2019/20 winter/spring season. Exceptionally low total ozone values of slightly less than 220 DU were observed in mid March within an unusually large stratospheric polar vortex.
This was associated with very low temperatures and extensive polar stratospheric cloud formation, a prerequisite for substantial springtime ozone depletion. Very high OClO and very low NO2 column amounts observed by GOME-2A are indicative of unusually large active chlorine levels and significant denitrification, which likely contributed to large chemical ozone loss. Using results from the TOMCAT chemical transport model (CTM) and ozone observations from S5P/TROPOMI, GOME-2 (total column), SCIAMACHY and OMPS-LP (vertical profiles) chemical ozone loss was evaluated and compared with the previous record Arctic winter 2010/11. The polar-vortex-averaged total column ozone loss in 2019/20 reached 88 DU (23%) and 106˜DU (28%) based upon observations and model, respectively, by the end of March, which was similar to that derived for 2010/11. The total column ozone loss is in agreement with OMPS-LP-derived partial column loss between 350 K and
550 K to within the uncertainty. The maximum ozone loss (˜80%) observed by OMPS-LP was near the 450 K potential temperature level (˜18 km altitude). Because of the larger polar vortex area in March 2020
compared to March 2011 (about 25% at 450 K), ozone mass loss was larger in Arctic winter 2019/20.

The unusual stratospheric Arctic winter 2019/20: Chemical ozone loss from satellite observations and TOMCAT chemical transport model

Mark Weber[1], Carlo Arosio[1], Wuhu Feng[2,3], Sandip S. Dhomse[2,4], Martyn P. Chipperfield[2,4], Andreas Meier[1], John P. Burrows[1], Kai-Uwe Eichmann[1], Andreas Richter[1], and Alexei Rozanov[1]

[1]Institute of Environmental Physics, University of Bremen, PO Box 330 440, D-28334 Bremen, Germany
[2]School of Earth and Environment, University of Leeds, Leeds, LS2 9JT, UK
[3]National Centre for Atmospheric Science, University of Leeds, Leeds, LS2 9PH, UK
[4]National Centre for Earth Observation, University of Leeds, Leeds, LS2 9JT, UK

Special section
The Exceptional Arctic Polar Vortex in 2019/2020: Causes and Consequences

Key Points:

- Very large OClO and very low NO_2 slant columns were observed by GOME-2A during Arctic winter 2019/20
- Chemical total column ozone loss of 88 DU and 106 DU was derived from TROPOMI satellite observations and the chemical transport model
- Chemical ozone loss derived from OMPS-LP satellite data reached 2.1 ppmv (80%) near the 450 K potential temperature level ($\sim$18 km)

Version
Monday 7[th] December, 2020, 13:51 UTC

Corresponding author: Mark Weber, `weber@uni-bremen.de`

Abstract

Satellite observations of relevant trace gases, together with meteorological data from ERA5, were used to describe the dynamics and chemistry of the spectacular Arctic 2019/20 winter/spring season. Exceptionally low total ozone values of slightly less than 220 DU were observed in mid March within an unusually large stratospheric polar vortex. This was associated with very low temperatures and extensive polar stratospheric cloud formation, a prerequisite for substantial springtime ozone depletion. Very high OClO and very low NO_2 column amounts observed by GOME-2A are indicative of unusually large active chlorine levels and significant denitrification, which likely contributed to large chemical ozone loss. Using results from the TOMCAT chemical transport model (CTM) and ozone observations from S5P/TROPOMI, GOME-2 (total column), SCIAMACHY and OMPS-LP (vertical profiles) chemical ozone loss was evaluated and compared with the previous record Arctic winter 2010/11. The polar-vortex-averaged total column ozone loss in 2019/20 reached 88 DU (23%) and 106 DU (28%) based upon observations and model, respectively, by the end of March, which was similar to that derived for 2010/11. The total column ozone loss is in agreement with OMPS-LP-derived partial column loss between 350 K and 550 K to within the uncertainty. The maximum ozone loss (~80%) observed by OMPS-LP was near the 450 K potential temperature level (~18 km altitude). Because of the larger polar vortex area in March 2020 compared to March 2011 (about 25% at 450 K), ozone mass loss was larger in Arctic winter 2019/20.

1 Introduction

While large springtime polar ozone depletion has been observed above Antarctica in most years since the 1980s (the "ozone hole"), such events occur only sporadically in the Arctic (Langematz et al., 2018). The chemistry involved in this depletion process is well understood (Solomon, 1999; Solomon et al., 2015). A prerequisite for substantial polar ozone depletion during winter/spring is sufficiently low stratospheric temperatures to form polar stratospheric clouds (PSCs) (e.g. Spang et al., 2018), which activate halogens, mainly chlorine, from their reservoir species. Sunlight returning to the polar region then allows rapid catalytic reactions involving the active halogens to destroy ozone.

Above Antarctica temperatures in the lower stratosphere are persistently below the PSC formation threshold. In contrast, above the Arctic such low temperatures are reached only sporadically and rarely persist over a long enough period to sustain the ozone depletion process. The strong variability in stratospheric meteorology, associated with variations in atmospheric dynamics, is responsible for the high variability in Arctic ozone and stratospheric temperatures due to enhanced ozone transport in warm winters and enhanced chemical loss in cold Arctic winters (e.g. Chipperfield & Jones, 1999; Tegtmeier et al., 2008; Weber et al., 2011; Strahan et al., 2016). The very low ozone observed in cold polar winters is therefore due to a combination of reduced transport and chemical loss (e.g. Weber et al., 2003; Tegtmeier et al., 2008).

The Arctic winter/spring 2019/20, along with 2010/11 and 1996/97 exhibited low stratospheric temperatures throughout February and well into March, associated with a deep depression in polar ozone in March resembling the Antarctic ozone hole (Lefèvre et al., 1998; Kuttippurath et al., 2012; Manney et al., 2011, 2020; Dameris et al., 2020; Lawrence et al., 2020) as shown in Fig. 1. In March 2020 total ozone was up to 200 DU lower than the year before. Arctic winter 2019/20, in particular, has some similarity to the winter 2010/11 (Manney et al., 2011) which, until now, showed the largest estimated ozone depletion.

In this paper we report on chemical ozone loss in Arctic winter 2019/20 derived from total ozone data from TROPOMI (TROPOspheric Monitoring Instrument) and ozone profiles from OMPS-LP (Ozone Mapping and Profiler Suite - Limb Profiler) satellite data

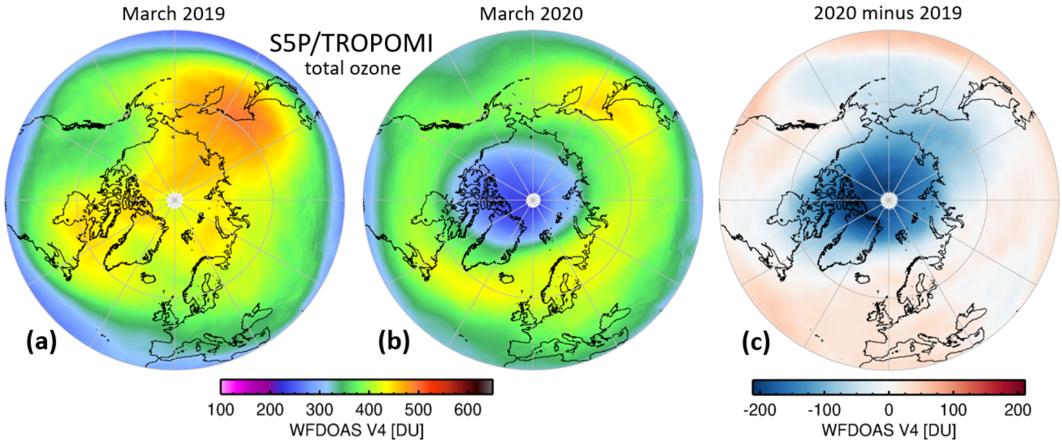

Figure 1. Arctic March mean total ozone (DU) from TROPOMI in (a) 2019 and (b) 2020, representative for years with average conditions and above-average-sized polar vortices, respectively. (c) Difference (DU) between mean March 2020 and 2019 total ozone. The total ozone was retrieved using WFDOAS (weighting function DOAS) V4.

in combination with results from the 3D chemical transport model (CTM) TOMCAT (Chipperfield, 2006). A particular focus in this paper is on the comparison between 2019/20 and the previous record winter 2010/11 for which ozone column data from GOME-2A (Global Ozone and Monitoring Experiment- Metop A) and limb data from SCIAMACHY (SCanning Imaging Absorption SpectroMeter for Atmospheric CHartographY) are also used.

The structure of this paper is as follows. Section 2 describes the observational data and CTM used here. Section 3 gives a brief description of the polar meteorology in the Arctic winter/spring 2019/2020, including a comparison to the record winter/spring in 2010/11. Section 4 shows results from other trace gas observations (NO_2 and OClO) along with ozone followed, in Section 5, by chemical ozone loss calculations using the combination of model and observational data. Our summary and concluding remarks are provided in Section 6.

2 Data

2.1 Merged WFDOAS total ozone

The merged GOME, SCIAMACHY, GOME-2, and TROPOMI (GSG) total ozone timeseries consists of total ozone data retrieved using an advanced version of the University of Bremen Weighting Function DOAS (WFDOAS) algorithm (Coldewey-Egbers et al., 2005; Orfanoz-Cheuquelaf et al., 2020). The merging of the various instruments has been briefly described in Weber et al. (2018). A monthly mean latitude-dependent bias correction, used to successively adjust SCIAMACHY (2002-2012) and GOME-2A (2007-present) to the initial GOME (1995-2011) data record, has been applied here to daily gridded data. Recently bias-adjusted WFDOAS data from GOME-2B (with a better global coverage than GOME-2A) starting in 2015 and TROPOMI (Veefkind et al., 2012) starting in 2018 have been added into the merged daily WFDOAS total ozone timeseries, available at a spatial resolution of $1.25° \times 1°$ (longitude $\times$ latitude).

2.2 SCIAMACHY and OMPS-LP ozone profiles

SCIAMACHY aboard Envisat (2002-2012) and OMPS-LP aboard SUOMI-NPP (2012-present) observe the atmosphere in limb geometry from a sun-synchronous orbit and collect radiances in the UV-VIS spectral region. Ozone concentrations are retrieved from 60 down to 10 km (or cloud top height), by using for both instruments the SCIATRAN radiative transfer model and retrieval software package (Rozanov et al., 2014). The typical vertical resolution of the retrieved profiles is about 2.5 km (OMPS-LP) and 3.7 km (SCIAMACHY). Details of the retrieval algorithm and a validation of the ozone profiles can be found in Jia et al. (2015) and Arosio et al. (2018).

2.3 GOME-2A OClO and NO_2 columns

Stratospheric OClO and NO_2 columns retrieved from UV/visible observations of instrument such as GOME and SCIAMACHY have already been used in previous studies (Wagner et al., 2001; Weber et al., 2003; Richter et al., 2005). Here, the data analysis follows Richter et al. (2005) but using GOME-2A data instead of GOME observations. Since OClO is rapidly photolyzed, substantial amounts can only be measured at very large solar zenith angles (SZA). In order to remove the effect of changing illumination during the time series, only observations at 90° SZA are used. As rapid photolysis also changes the OClO concentration along the light path, no attempt is made to convert OClO slant columns into vertical columns. As the geometry of the light path remains the same for all measurements at 90° SZA, the results are still comparable from day to day and between years.

The variations in local equator crossing times (and twilight zones at a given day of the year) of the various satellites complicate the comparison between satellites. For this reason, we limit our comparisons to results from the GOME-2A instrument (launched in 2006) that covers both cold Arctic winters studied here. As a result of the sun-synchronous orbit of GOME-2A, the latitude probed at 90° SZA varies from 65° to 85° over the winter / spring period, and does not reflect vortex or polar-cap averages as the ozone data used here.

2.4 TOMCAT chemical transport model

TOMCAT/SLIMCAT (hereafter TOMCAT) is a 3-D chemical transport model (CTM), which has been described in Dhomse et al. (2019). The model contains a detailed description of stratospheric chemistry, including heterogeneous reactions on sulfate aerosols and PSCs. Here the model was forced using European Centre for Medium-Range Weather Forecasts (ECMWF) ERA5 winds and temperatures (Hersbach et al., 2020) and run with a horizontal resolution of $2.8° \times 2.8°$ with 32 altitude levels from the surface to ~60 km. The run was initialised in 1977 and forced using specified surface mixing ratios of the long-lived source gases. In recent model updates the supersaturation of HNO_3 for type I PSC formation was implemented according to Grooß et al. (2018) and the Cl_2O_2 absorption cross sections are from Burkholder et al. (2015) with an assumed quantum yield of 1. Solar flux variations [1980–2019] are taken from the NRLSSI2 empirical model (Coddington et al., 2016) that are recommended for CMIP6 simulations as implemented in Dhomse et al. (2016). For the year 2020, solar fluxes are held constant at December 2019 values.

2.5 ERA5 Reanalysis

Wind and temperature data from the ERA5 re-analysis (Hersbach et al., 2020) are used here for determining dynamical properties (vortex and PSC volume) and driving the TOMCAT CTM. For the polar vortex diagnostics 6-hourly data at a spatial resolution of $0.75° \times 0.75°$ were used.

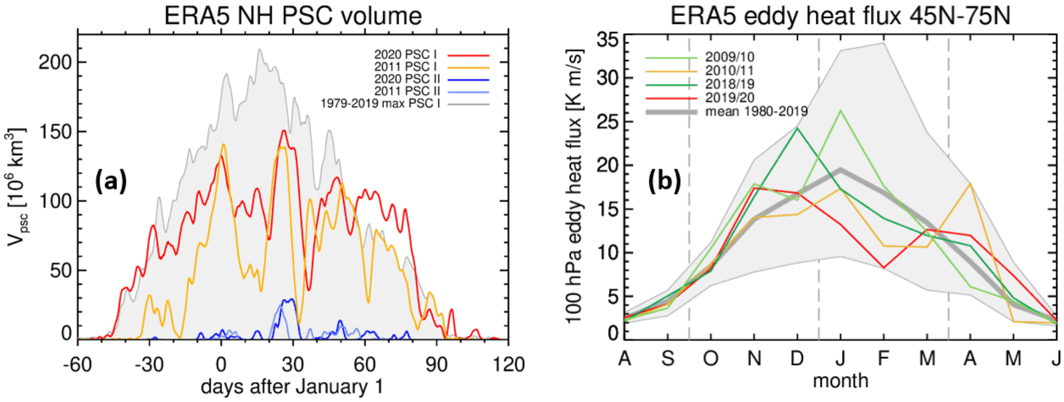

Figure 2. (a) Type I and type II PSC volume ($\times 10^6$ km^3) in Arctic winters 2010/11 and 2019/20 derived from ERA5 reanalysis in the potential temperature range 400 to 750 K. The grey shading indicates the maximum values of type I PSC volume from 1979 to spring 2019. All curves have been smoothed with a running [1,2,1] triangular filter. (b) Monthly mean ERA5 100 hPa eddy heat flux integrated between 45°N and 75°N.

3 Meteorology

The Arctic winter/spring 2019/20 exhibited a strong polar vortex with persistent PSCs observed from mid November until April, as shown in Fig. 2. Here the PSC volume was calculated using ERA5 data at potential temperature levels in order to identify grid boxes with temperatures below the PSC formation threshold as described in Feng et al. (2007). PSC volumes were derived in steps of 25 K potential temperature from 400 K to 750 K altitudes. For the vertical extent it was assumed that 25 K roughly corresponds to 1 km altitude (Knox, 1998).

In Arctic winter 2019/20 the PSC volume was at a record high since 1979 in the second half of November. It remained high throughout December and January and was again at a record high in the second half of February through to nearly the end of March. The early PSC formation (chlorine activation) and very high PSC volumes in March, as shown in Fig. 2a, favoured strong depletion in ozone. The previous record winter 2010/11 showed a similar evolution in the volume of type I and type II PSCs as this year, with the exception that the volumes were generally smaller in 2011 and PSCs started to form later (end of November). Temporary lows in PSC volume had a very similar timing in both winters with local minima observed in the middle of January and a sharp short-term drop in early February, most likely related to minor stratospheric warming events perturbing the polar vortex. Maximum PSC volumes were reached at the end of January in both winters. At that time type II (ice) PSCs were also maximum in both winters. Ice PSCs can lead to strong dehydration and removal of water vapour that may result in a delay in deactivating active chlorine into HCl in early spring (Manney et al., 2020).

Fig. 2b shows northern hemisphere (NH) monthly mean eddy heat fluxes at 100 hPa for the two cold Arctic winters considered here, along with data from their preceding winters 2009/10 and 2018/19, respectively. The eddy heat flux is a measure of the planetary wave activity determining the strength of dynamical activity (ozone transport, driver of the Brewer-Dobson circulation) and stratospheric meteorology. From January to March the eddy heat flux was persistently below the long-term mean in both 2010/11 and 2019/20, resulting in reduced ozone transport as well as lower stratospheric temperatures (Newman et al., 2001; Randel et al., 2002; Weber et al., 2011). In February 2020 the 100 hPa eddy heat flux reached the lowest value since 1980, which may have been responsible for setting record high PSC volumes starting by the end of February 2020. Both the continuous low dynamical activity, also linked to the positive anomaly in the Arctic Oscillation (Lawrence et al., 2020), and very low stratospheric temperatures contributed to the very low ozone in Arctic winter 2019/20.

Further details on the stratospheric meteorology in this particular winter and comparisons to past winters can be found in this journal's special issue and other studies (Dameris et al., 2020; Inness et al., 2020; Lawrence et al., 2020; Manney et al., 2020).

4 Trace gas observations

The evolution of ozone, NO_2, and OClO, above the Arctic in 2019/20 are displayed in Fig. 3. Corresponding timeseries for the year 2010/11 (previous record winter) as well as the years preceding both cold winters, 2009/10 and 2018/19, with more typical conditions are also shown to demonstrate the large variability from year-to-year. Panel (a) shows the evolution of the polar cap mean total ozone (50°N-90°N). Due to the Brewer-Dobson circulation, total ozone normally increases over the winter reaching, on average, an annual maximum in March (thick grey curve). Starting in mid February, however, polar ozone strongly declined in 2011 and 2020. In mid March polar-cap mean were the lowest in both winters since the mid 1990s (since start of the WFDOAS merged total ozone timeseries), a time when stratospheric halogens originating from man-made ozone depleting substances (ODSs) were maximum (Newman et al., 2007). In 2020 the polar cap mean remained very low from March until May.

The polar minimum total ozone evolved in a a very similar way to the mean (Fig. 3b). A first record minimum was observed in March 2011 and this record was broken again in March 2020 with total ozone being slightly below 220 DU for a brief period (Inness et al., 2020; Wohltmann et al., 2020), a value which commonly defines the boundary of the Antarctic ozone hole (e.g. *NASA Ozone Watch*, 2020). The steady decline in minimum ozone in polar winter is considered a good proxy for continued polar chemical ozone loss (Müller et al., 2008). The rapid declines and rises in minimum ozone observed in early November and late January 2020 are, in contrast, purely dynamical in nature. They are caused by subtropical streamers intruding into polar latitudes producing so-called ozone mini holes by fast horizontal advection of ozone away from a region with a strongly elevated tropopause (James et al., 2000; Weber et al., 2002; Dameris et al., 2020).

In both Arctic winters 2010/11 and 2019/20 the mean NO_2 and OClO slant columns were record minima and maxima, respectively, by late February and early March (Fig. 3c,d). In particular, OClO levels reached a new record (since 2007) in March 2020, which indicates substantial chlorine activation up to the last measurements mid of March. After that, the sun is too high for GOME-2A measurement at 90° SZA and the time series ends before the end of chlorine activation is reached.

Stratospheric NO_2 levels are generally small in the winter polar regions as most NO_2 is converted into its night-time reservoirs (N_2O_5 and HNO_3) during polar night (e.g. Burrows et al., 1999). As the sun returns to the Arctic, NO_2 levels usually increase through mixing of polar air masses with mid-latitude air and destruction of HNO_3 by photolysis and reaction with OH. A stable vortex and denitrification by subsidence of condensed HNO_3 in PSCs delay this process as well as subsequent deactivation of active chlorine into their reservoir species ($ClONO_2$), explaining both the low NO_2 columns and the extended chlorine activation observed in 2011 and 2020.

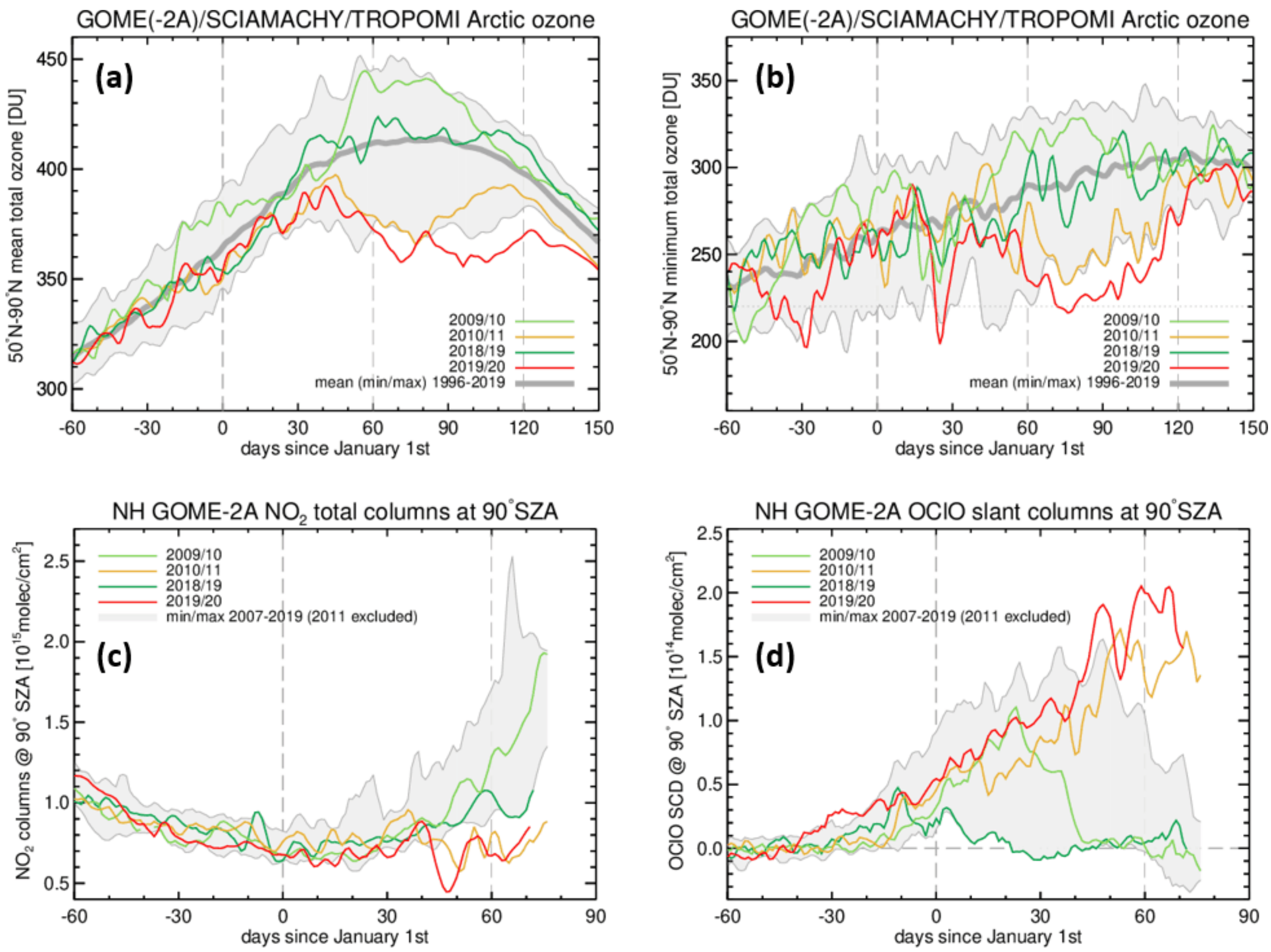

Figure 3. Time series of Arctic polar cap (50°N-90°N) (a) mean total ozone (DU), (b) minimum total ozone (DU), (c) mean NO_2 and (d) mean OClO. Panels (c) and (d) show mean 90° solar zenith angle (SZA) column densities (total columns) of NO_2 and 90° SZA slant column densities (SCD) of OClO, respectively. Selected years are shown by coloured lines, the two cold Arctic winters 2010/11 and 2019/20 and the two years (2009/10 and 2018/19) preceding both cold winters. Daily minimum total ozone columns shown here are averages of the ten grid boxes (1° × 1.25°) with the lowest total ozone. The grey shading provides the range of maximum and minimum values since 1995 (ozone) and 2007 (minor trace gases), respectively. The thick grey lines in the ozone panels show the long-term mean since 1995. All curves have been smoothed with a running [1,2,1] triangular filter.

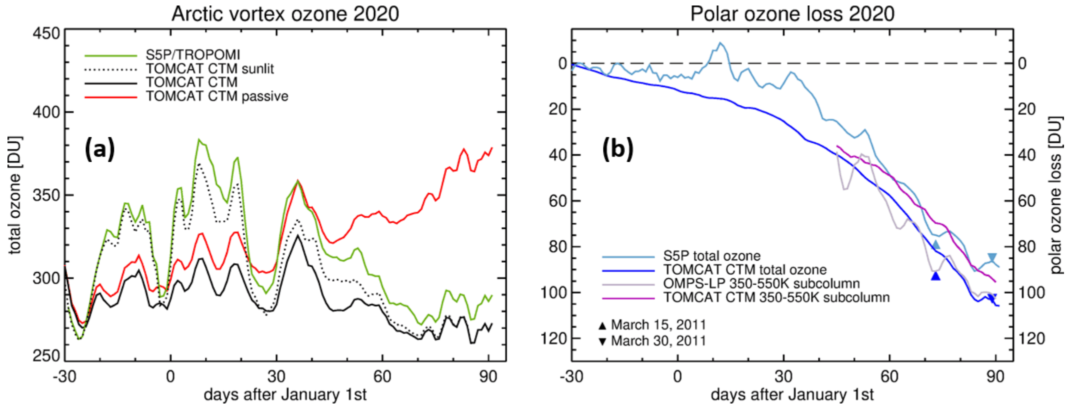

Figure 4. Evolution of Arctic vortex-mean (a) total ozone (DU) and (b) chemical ozone loss (DU) in winter 2019/20. In panel (a) timeseries of TROPOMI (green) and TOMCAT (black) are shown. Dotted black line is TOMCAT data limited to the sunlit part of the polar vortex, while the red line displays the passive ozone from TOMCAT. The vortex area was determined here for the 450 K surface. In panel (b) the light blue line represents the ozone loss derived from TROPOMI using TOMCAT passive ozone (see main text for explanations). Dark blue line shows the TOMCAT-derived column ozone loss. For comparisons triangles show the total column ozone losses from the observations and the model on March 15 and 30 in 2011, respectively. Also shown in panel (b) are the partial column ozone losses (350 K-550 K altitude) from OMPS-LP and TOMCAT.

5 Chemical ozone loss

The chemical ozone loss in both cold Arctic winters 2010/11 and 2019/20 is estimated using the vortex-average approach (Harris et al., 2002). In this approach total ozone and ozone profiles are averaged daily within the confines of the polar vortex and the difference to a passive ozone tracer, here from the TOMCAT CTM, is considered as the accumulated ozone loss. The vortex edge is here defined by the combination of maximum wind speed and potential vorticity (PV) gradient (Nash et al., 1996) and was determined at the 450 K potential temperature level. The timeseries of vortex-averaged total ozone from TROPOMI and TOMCAT are shown in Fig. 4 for the winter 2019/20. The same quantities for the winter 2010/11 are displayed in Fig. 5 using observations from GOME-2A and SCIAMACHY. While panel (a) shows the various timeseries over the course of the winter, corresponding polar ozone losses are displayed in panel (b). The TOMCAT vortex-averaged ozone has evidently a negative bias with respect to TROPOMI, which is particularly large in the middle of the winter, which may be partly due to the strong descent in the model forced by the ERA5 reanalysis.

TROPOMI, OMPS-LP (and SCIAMACHY) measure in the optical range and thus do not observe the polar night region, such that the polar vortex is usually only covered by 10 to 20%, depending on its exact location, in late December and early January. The agreement between observations and model improves significantly when using model averages from the sunlit part of the polar vortex only (dotted line in Fig. 4a). In the beginning of December the observations agree well with the model, but the bias increases with time until the end of March (when the polar vortex is completely illuminated) indicating that modelled ozone loss is slightly larger than that observed (by ∼15 DU). The observed ozone loss is here approximated by subtracting the difference between observations (green curve) and the sunlit part of the model ozone (dotted line) from the modelled ozone loss. Alternatively, one could also have taken the difference between the sun-

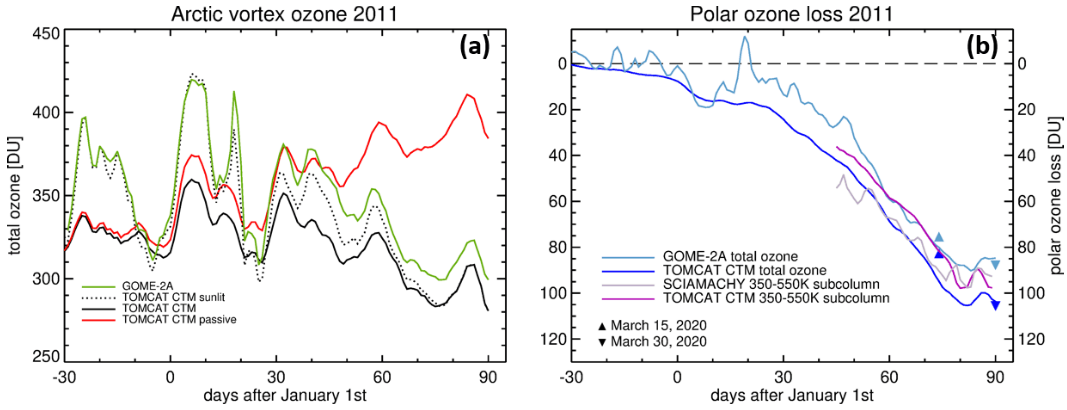

Figure 5. Same as Fig. 4 but for winter 2010/11. Triangles show for comparison the total column ozone loss on March 15 and March 30 in 2020. Here observational data from GOME-2A (total column) and SCIAMACHY (subcolumns) are shown.

lit part of modelled passive ozone and observations. One important assumption for both alternatives of the observed ozone loss calculation here is that the negligible difference between passive ozone and satellite observations in the sunlit part of the polar vortex ozone in early December also holds for the entire polar vortex. The estimated observed chemical loss curve is thus not necessarily representative for the entire polar vortex in early winter but approaches the full vortex value by late March.

By the end of March 2020 the TROPOMI accumulated total ozone loss amounts to 88 DU (23%) and for the TOMCAT CTM to 106 DU (28%). These losses are quite similar to the results from the previous record winter 2010/11 as indicated by the triangles in Fig. 4b (see also Fig. 5). On March 15, where observed minimum total ozone is near its lowest value (Fig. 2b) the mean total ozone loss is even slightly higher in 2011 than 2020, for both observations and CTM.

Fig. 6 shows the time series of March daily mean vortex-averaged ozone profiles from SCIAMACHY (2011) and OMPS-LP (2020). Only profiles with a PV value higher than 38 PVU (at 475 K) were averaged to obtain the daily Arctic vortex mean. The rapid decline of ozone near 450 K potential temperature levels throughout March is clearly evident. It appears that the largest decline in 2020 was slightly below 450 K, a bit lower than in 2011 apparently in agreement with Microwave Limb Sounder (MLS) observations reported in Manney et al. (2020). However, one needs to be cautious here as the vertical sampling of SCIAMACHY (3.3 km $\approx$ 75 K) is too coarse to clearly support this.

Figure 7 shows a time-altitude cross-section of the accumulated ozone loss from SCIAMACHY (2010/11) and OMPS-LP (2019/20). Similar to total ozone, the ozone loss here is calculated from the difference of the daily mean observed ozone profiles to the passive ozone from TOMCAT. For this purpose, only TOMCAT profiles collocated with SCIAMACHY / OMPS-LP observations are considered. Passive ozone is initiated in the model on December 1 each Arctic winter. A comparison between observations and passive ozone in early December, a period where chemical ozone loss is still very small, revealed differences of about 12 DU (2010) and 21 DU (2019) in the 350-550 K column which are accounted for in the ozone loss shown in Fig. 7. By the end of March 2020 a maximum ozone loss of 2.1 ppmv near 450 K was observed. In 2011 the accumulated loss reached a maximum of 2.2 ppmv which is comparable to the value from 2020. These values are slightly smaller than, but in good agreement with, Manney et al. (2011, 2020), confirming that the ozone losses observed in both winters were at a record low.

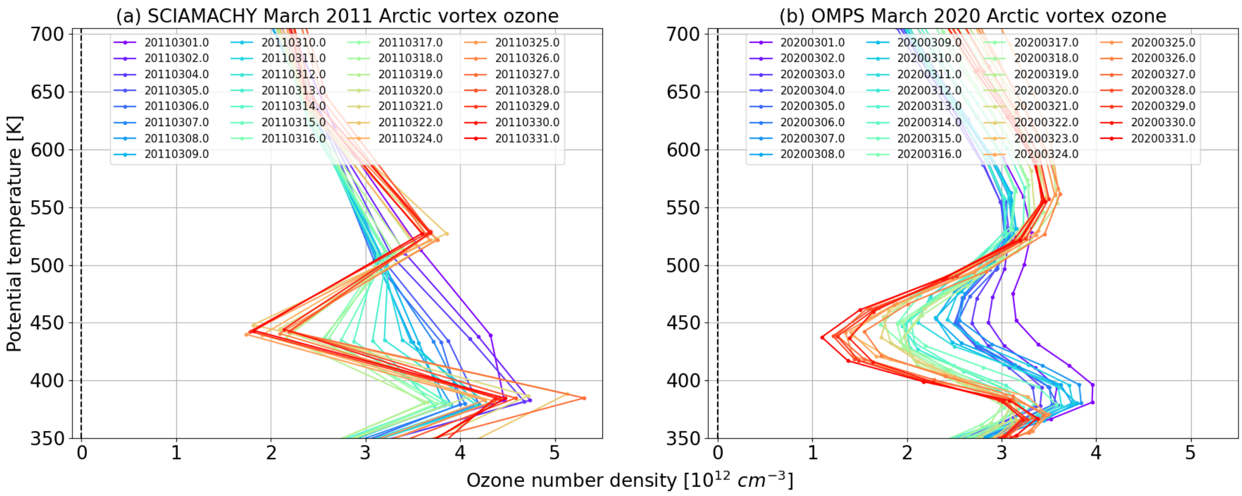

Figure 6. March sequence of daily mean Arctic vortex ozone profiles as a function of potential temperature from (a) SCIAMACHY in 2011 and (b) OMPS-LP in 2020. Colors indicate individual dates as provided in the legend. The Arctic vortex region was here determined from the 475 K altitude level.

Since most of the ozone decrease occurs between 350 and 550 K, subcolumn ozone loss values were derived from the profile observations and CTM. The subcolumn (350-550 K) ozone loss is displayed along with the total ozone data in Figs. 4b and 5b. The OMPS-LP subcolumn ozone loss is 105 DU, about 20 DU larger than the TROPOMI total column ozone loss at the end of March 2020. The modelled subcolumn loss on the other hand (95 DU) is closer to the observation-derived total column loss of 88 DU. In 2011 the observation-derived and modelled subcolumn ozone loss at the end of March 2011 differ slightly by 5 DU. The largest error in the estimated ozone loss comes from uncertainties in establishing a proper initial Arctic vortex-mean ozone value from the UV/visible observations as well as uncertainties in the CTM, e.g. vertical transport in the polar vortex and uncertainties in photochemical data propagating into uncertainties in the model chemistry. The overall uncertainty in the established polar ozone loss is estimated to be about 15% (about 15 DU). Nevertheless, both CTM and observations agree that Arctic vortex-averaged ozone losses in both Arctic winters 2011 and 2020 were very similar.

The product of mean column ozone loss and average vortex area provides an estimate of the total number of ozone molecules lost (which is proportional to the ozone mass loss). At 450 K the vortex area was, on average, about 20 million square km, about 4 million square km larger than in 2011 (see also Fig. 10a in Lawrence et al. (2020)). As a consequence, the mass loss in ozone was about 25% larger in 2020 compared to 2011 assuming a similar vortex-averaged column ozone loss in both winters. In terms of ozone mass loss the Arctic winter 2019/20 therefore sets a new record high.

6 Summary and conclusions

The Arctic winter/spring 2019/20 is one of the coldest on record (Lawrence et al., 2020; Dameris et al., 2020; Inness et al., 2020) with temperatures sufficient for PSC occurrence from November until April. The PSC volume was at a record high (based on available observations) in November and from late February throughout March, which indicates substantial polar ozone loss. OClO slant columns were very high and NO_2 slant

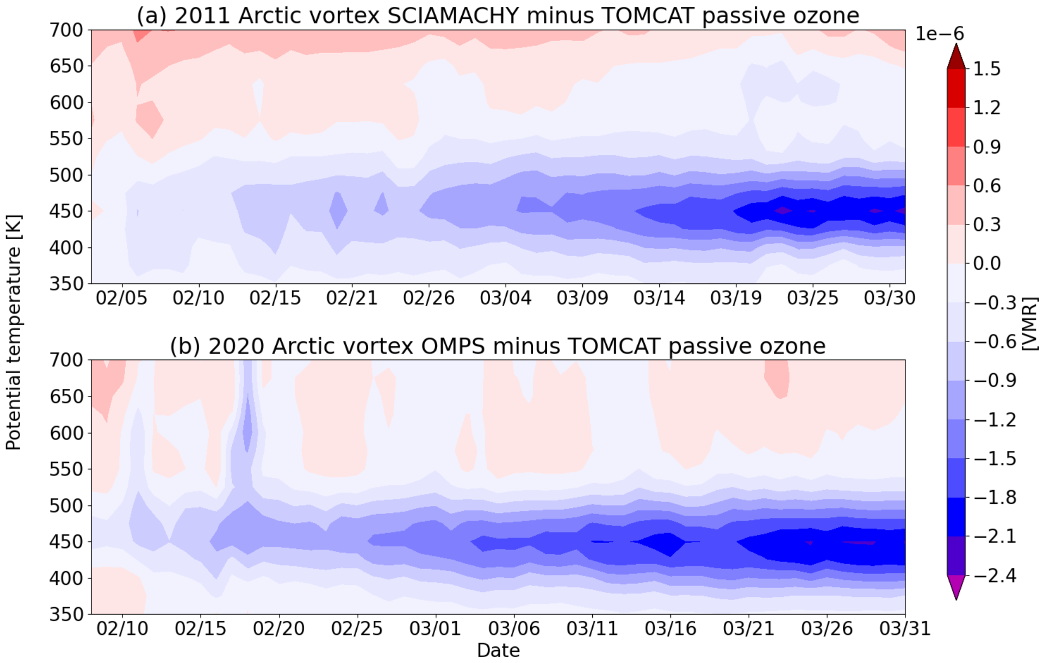

Figure 7. Time-altitude cross-section of estimated ozone loss in late Arctic winter and early spring (a) from SCIAMACHY in 2011 and (b) from OMPS-LP in 2020. The daily ozone loss was determined from the difference between Arctic vortex-mean passive ozone profile from TOMCAT and observed ozone profiles. Biases in passive ozone with respect to observations in early December have been corrected for in the loss calculations (see main text). Vortex area is derived here at the 475 K altitude level.

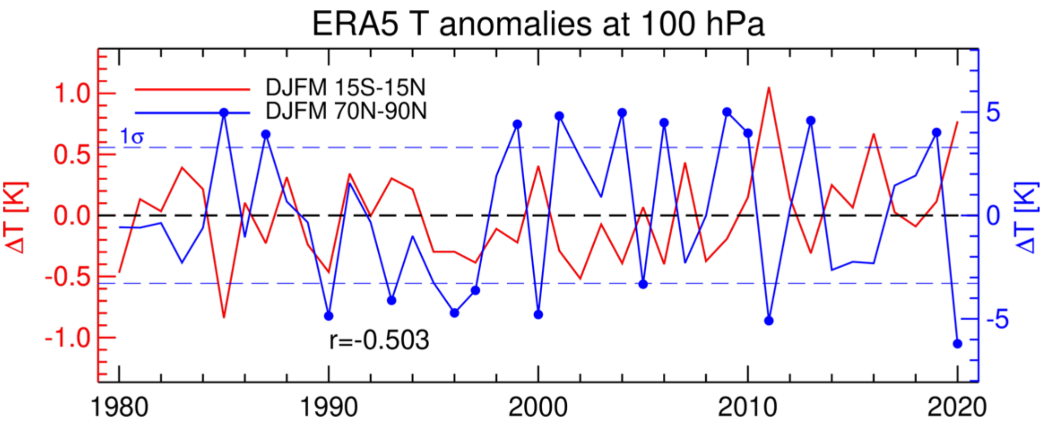

Figure 8. ERA5 100 hPa polar-cap (blue) and tropical temperature (red) timeseries from 1980 to 2020. Blue dots indicate mean polar temperature anomalies outside the 1σ standard deviation of the long-term mean indicated by the two blue dashed lines.

columns very low in February and March, indicating large chlorine activation and extensive denitrification, both consistent with continued chemical ozone losses well into early spring. In February 2020 the planetary wave activity was at a record low resulting in very low temperatures in February and March and record high PSC volume.

Using total ozone observations from TROPOMI and TOMCAT/SLIMCAT model simulations, the total column ozone loss was estimated to be 88 DU and 106 DU, respectively, by the end of March (23-28% loss). From OMPS-LP observations ozone profile losses were found to reach 2.1 ppmv at 450 K (∼18 km) in good agreement with MLS observations (Manney et al., 2020). The combined uncertainty of derived polar ozone loss (from model and observations) is estimated to be on the order of 15%. The vortex-averaged ozone loss was very similar in both Arctic winters 2010/11 and 2019/20, but the ozone mass loss was significantly higher (about 25%) in 2020 than 2011 due to the larger area of the Arctic vortex in March 2020.

An important question concerns the reason behind such a large ozone loss observed in winter 2019/20, given the fact that ODSs are mostly declining as a consequence of the Montreal Protocol and Amendments. While in the Antarctic first signs of ozone recovery have been detected (Solomon et al., 2016; de Laat et al., 2017; Weber et al., 2018), the variability in stratospheric meteorology and ozone in the Arctic is still too large to uniquely identify ozone recovery (e.g. Chipperfield et al., 2017; Dhomse et al., 2018). CTM calculations, however, show that the ozone loss would have been larger in 2019/20 with ODS at levels of the mid 1990s (Feng et al., 2020).

The Arctic winter 2019/20 exhibited record-low polar-cap temperature at 100 hPa based upon ERA5 reanalysis data as shown in Fig. 8. Although most Arctic winters were rather warm (above 1σ variability) after the mid 1990s, about two winters in a decade were extremely cold. The hypothesis discussed for some time that cold Arctic winters are getting colder in a changing climate (Rex et al., 2004, 2006; Rieder & Polvani, 2013) gains new relevance after the record temperatures observed in 2019/20. Also shown in Fig. 8 are tropical 100 hPa temperatures during boreal winter, displaying an anti-correlation with polar-cap temperatures (Yulaeva et al., 1994). This correlation is a result of the inter-annual variability in the Brewer-Dobson circulation (weak circulation associated with higher tropical upper troposphere - lower stratosphere (UTLS) temperatures due to weaker vertical ascent in the tropics).

The two unusual cold Arctic winters of the past decade fall in a period where a weak positive tropical temperature trend is apparent. This suggests that a slight weakening of the Brewer-Dobson circulation, opposite to the expected long-term trend from climate change (e.g. Aschmann et al., 2014; Garfinkel et al., 2017), may have contributed to these two recent extreme Arctic winters.

Acknowledgments

ERA5 reanalysis were made available to U. Bremen by ECMWF via a data agreement with the German Weather Service (DWD). WF, SSD and MPC are grateful for access to the ERA5 data. Daily data from the GSG merged total ozone data are available from `http://www.iup.uni-bremen.de/UVSAT/datasets/merged-wfdoas-total-ozone`. Part of the data processing was done at the German HLRN (High Performance Computer Center North). SCIAMACHY and OMPS-LP limb ozone profile data as well as GOME-2A minor trace gas data are available at `https://www.iup.uni-bremen.de/DataRequest/`. The model simulations were performed on the UK national Archer and Leeds Arc4 HPC systems. The financial support of part of this work from the State of Bremen, DAAD grant (CA), and ESA SOLVE Living Planet Fellowship (CA) is gratefully acknowledged.

References

Arosio, C., Rozanov, A., Malinina, E., Eichmann, K.-U., von Clarmann, T., & Burrows, J. P. (2018). Retrieval of ozone profiles from OMPS limb scattering observations. *Atmospheric Measurement Techniques*, *11*, 2135–2149. doi: 10.5194/amt-11-2135-2018

Aschmann, J., Burrows, J. P., Gebhardt, C., Rozanov, A., Hommel, R., Weber, M., & Thompson, A. M. (2014). On the hiatus in the acceleration of tropical upwelling since the beginning of the 21st century. *Atmospheric Chemistry and Physics*, *14*, 12803–12814. doi: 10.5194/acp-14-12803-2014

Burkholder, J. B., Sander, S. P., Abbatt, J. P. D., Barker, J. R., Huie, R. E., Kolb, C. E., … Wine, P. H. (2015). *Chemical Kinetics and Photochemical Data for Use in Atmospheric Studies - Evaluation Number 18.* Pasadena, CA, USA. Retrieved from `https://jpldataeval.jpl.nasa.gov/pdf/JPL_Publication_15-10.pdf`

Burrows, J. P., Weber, M., Buchwitz, M., Rozanov, V., Ladstätter-Weißenmayer, A., Richter, A., … Perner, D. (1999). The Global Ozone Monitoring Experiment (GOME): Mission Concept and First Scientific Results. *Journal of the Atmospheric Sciences*, *56*, 151–175. doi: 10.1175/1520-0469(1999)056⟨0151:TGOMEG⟩2.0.CO;2

Chipperfield, M. P. (2006). New version of the TOMCAT/SLIMCAT off-line chemical transport model: Intercomparison of stratospheric tracer experiments. *Quarterly Journal of the Royal Meteorological Society*, *132*, 1179–1203. doi: 10.1256/qj.05.51

Chipperfield, M. P., Bekki, S., Dhomse, S., Harris, N. R. P., Hassler, B., Hossaini, R., … Weber, M. (2017). Detecting recovery of the stratospheric ozone layer. *Nature*, *549*, 211–218. doi: 10.1038/nature23681

Chipperfield, M. P., & Jones, R. L. (1999). Relative influences of atmospheric chemistry and transport on Arctic ozone trends. *Nature*, *400*, 551–554. doi: 10.1038/22999

Coddington, O., Lean, J. L., Pilewskie, P., Snow, M., & Lindholm, D. (2016). A Solar Irradiance Climate Data Record. *Bulletin of the American Meteorological Society*, *97*, 1265–1282. doi: 10.1175/BAMS-D-14-00265.1

Coldewey-Egbers, M., Weber, M., Lamsal, L. N., de Beek, R., Buchwitz, M., & Burrows, J. P. (2005). Total ozone retrieval from GOME UV spectral data using the weighting function DOAS approach. *Atmospheric Chemistry and Physics*, *5*, 1015–1025. doi: 10.5194/acp-5-1015-2005

Dameris, M., Loyola, D. G., Nützel, M., Coldewey-Egbers, M., Lerot, C., Romahn, F., & van Roozendael, M. (2020). First description and classification of the ozone hole over the arctic in boreal spring 2020. *Atmospheric Chemistry and Physics Discussions*, *2020*, 1–26. Retrieved from `https://acp.copernicus.org/preprints/acp-2020-746/`

de Laat, A. T. J., van Weele, M., & van der A, R. J. (2017). Onset of Stratospheric Ozone Recovery in the Antarctic Ozone Hole in Assimilated Daily Total Ozone Columns. *Journal of Geophysical Research: Atmospheres*, *122*, 11,880–11,899. doi: 10.1002/2016JD025723

Dhomse, S. S., Chipperfield, M. P., Damadeo, R. P., Zawodny, J. M., Ball, W. T., Feng, W., ... Haigh, J. D. (2016). On the ambiguous nature of the 11-year solar cycle signal in upper stratospheric ozone. *Geophysical Research Letters*, *43*(13), 7241-7249. doi: 10.1002/2016GL069958

Dhomse, S. S., Feng, W., Montzka, S. A., Hossaini, R., Keeble, J., Pyle, J. A., ... Chipperfield, M. P. (2019). Delay in recovery of the Antarctic ozone hole from unexpected CFC-11 emissions. *Nature Communications*, *10*, 5781. doi: 10.1038/s41467-019-13717-x

Dhomse, S. S., Kinnison, D., Chipperfield, M. P., Salawitch, R. J., Cionni, I., Hegglin, M. I., ... Zeng, G. (2018). Estimates of ozone return dates from Chemistry-Climate Model Initiative simulations. *Atmospheric Chemistry and Physics*, *18*, 8409–8438. doi: 10.5194/acp-18-8409-2018

Feng, W., Chipperfield, M. P., Davies, S., von der Gathen, P., Kyrö, E., Volk, C. M., ... Belyaev, G. (2007). Large chemical ozone loss in 2004/2005 Arctic winter/spring. *Geophysical Research Letters*, *34*. doi: 10.1029/2006GL029098

Feng, W., Dhomse, S., Arosio, C., Weber, M., Burrows, J. P., Santee, M. L., & Chipperfield, M. P. (2020). Arctic ozone depletion in 2019/20: Roles of chemistry, dynamics and the Montreal Protocol. *Earth and Space Science Open Archive*, 15. doi: 10.1002/essoar.10505119.1

Garfinkel, C. I., Aquila, V., Waugh, D. W., & Oman, L. D. (2017). Time-varying changes in the simulated structure of the Brewer–Dobson Circulation. *Atmospheric Chemistry and Physics*, *17*, 1313–1327. doi: 10.5194/acp-17-1313-2017

Grooß, J.-U., Müller, R., Spang, R., Tritscher, I., Wegner, T., Chipperfield, M. P., ... Madronich, S. (2018). On the discrepancy of HCl processing in the core of the wintertime polar vortices. *Atmospheric Chemistry and Physics*, *18*, 8647–8666. doi: 10.5194/acp-18-8647-2018

Harris, N. R. P., Rex, M., Goutail, F., Knudsen, B. M., Manney, G. L., Müller, R., & von der Gathen, P. (2002). Comparison of empirically derived ozone losses in the Arctic vortex. *Journal of Geophysical Research*, *107*, 8264. doi: 10.1029/2001JD000482

Hersbach, H., Bell, B., Berrisford, P., Hirahara, S., Horányi, A., Muñoz-Sabater, J., ... Thépaut, J. (2020). The ERA5 global reanalysis. *Quarterly Journal of the Royal Meteorological Society*, *146*, 1999–2049. doi: 10.1002/qj.3803

Inness, A., Chabrillat, S., Flemming, J., Huijnen, V., Langenrock, B., Nicolas, J., ... Razinger, M. (2020). The unusual 2020 arctic ozone hole as seen in the cams reanalysis. *Earth and Space Science Open Archive*, 25. doi: 10.1002/essoar.10503751.1

James, P. M., Peters, D., & Waugh, D. W. (2000). Very low ozone episodes due to polar vortex displacement. *Tellus B: Chemical and Physical Meteorology*, *52*, 1123–1137. doi: 10.3402/tellusb.v52i4.17089

Jia, J., Rozanov, A., Ladstätter-Weißenmayer, A., & Burrows, J. P. (2015). Global validation of SCIAMACHY limb ozone data (versions 2.9 and 3.0, IUP Bremen) using ozonesonde measurements. *Atmospheric Measurement Techniques*, *8*, 3369–3383. doi: 10.5194/amt-8-3369-2015

Knox, J. A. (1998). On converting potential temperature to altitude in the middle atmosphere. *Eos, Transactions American Geophysical Union*, *79*, 376–378. doi: 10.1029/98EO00290

Kuttippurath, J., Godin-Beekmann, S., Lefèvre, F., Nikulin, G., Santee, M. L., & Froidevaux, L. (2012). Record-breaking ozone loss in the Arctic winter 2010/2011: comparison with 1996/1997. *Atmospheric Chemistry and Physics*, *12*, 7073–7085. doi: 10.5194/acp-12-7073-2012

Langematz, U., Tully, M. B., Calvo, N., Dameris, M., de Laat, A. T. J., Klekociuk, A., ... Young, P. (2018). Update on Polar Stratospheric Ozone: Past, Present, and Future. In *Scientific assessment of ozone depletion: 2018, world meteorological organization, global ozone research and monitoring project - report no. 58* (chap. 4). World Meteorological Organization/UNEP. Retrieved from `https://public.wmo.int/en/resources/library/scientific-assessment-of-ozone-depletion-2018`

Lawrence, Z. D., Perlwitz, J., Butler, A. H., Manney, G. L., Newman, P. A., Lee, S. H., & Nash, E. R. (2020). The remarkably strong Arctic stratospheric polar vortex of winter 2020: Links to record-breaking Arctic Oscillation and ozone loss. *Journal of Geophysical Research: Atmospheres*. doi: 10.1029/2020JD033271

Lefèvre, F., Figarol, F., Carslaw, K. S., & Peter, T. (1998). The 1997 Arctic Ozone depletion quantified from three-dimensional model simulations. *Geophysical Research Letters*, *25*, 2425–2428. doi: 10.1029/98GL51812

Manney, G. L., Livesey, N. J., Santee, M. L., Froidevaux, L., Lambert, A., Lawrence, Z. D., ... Fuller, R. A. (2020). Record-low Arctic stratospheric ozone in 2020: MLS observations of chemical processes and comparisons with previous extreme winters. *Geophysical Research Letters*, *47*. doi: 10.1029/2020GL089063

Manney, G. L., Santee, M. L., Rex, M., Livesey, N. J., Pitts, M. C., Veefkind, P., ... Zinoviev, N. S. (2011). Unprecedented Arctic ozone loss in 2011. *Nature*, *478*, 469–475. doi: 10.1038/nature10556

Müller, R., Grooß, J.-U., Lemmen, C., Heinze, D., Dameris, M., & Bodeker, G. (2008). Simple measures of ozone depletion in the polar stratosphere. *Atmospheric Chemistry and Physics*, *8*, 251–264. doi: 10.5194/acp-8-251-2008

NASA Ozone Watch. (2020). `https://ozonewatch.gsfc.nasa.gov/facts/hole_SH.html`. (Accessed: 2020-11-16)

Nash, E. R., Newman, P. A., Rosenfield, J. E., & Schoeberl, M. R. (1996). An objective determination of the polar vortex using Ertel's potential vorticity. *Journal of Geophysical Research: Atmospheres*, *101*, 9471–9478. doi: 10.1029/96JD00066

Newman, P. A., Daniel, J. S., Waugh, D. W., & Nash, E. R. (2007). A new formulation of equivalent effective stratospheric chlorine (EESC). *Atmospheric Chemistry and Physics*, *7*, 4537–4552. doi: 10.5194/acp-7-4537-2007

Newman, P. A., Nash, E. R., & Rosenfield, J. E. (2001). What controls the temperature of the Arctic stratosphere during the spring? *Journal of Geophysical Research: Atmospheres*, *106*, 19999–20010. doi: 10.1029/2000JD000061

Orfanoz-Cheuquelaf, A., Rozanov, A., Weber, M., Arosio, C., Ladstätter-Weißenmayer, A., & Burrows, J. P. (2020). *WFFA total ozone column retrieval from OMPS-NM/NPP.* (to be submitted to Atmospheric Measurement Techniques)

Randel, W. J., Wu, F., & Stolarski, R. (2002). Changes in column ozone correlated with the stratospheric EP flux. *Journal of the Meteorological Society of Japan*, *80*, 849–862. doi: 10.2151/jmsj.80.849

Rex, M., Salawitch, R. J., Deckelmann, H., von der Gathen, P., Harris, N. R. P., Chipperfield, M. P., ... Zerefos, C. (2006). Arctic winter 2005: Implications for stratospheric ozone loss and climate change. *Geophysical Research Letters*, *33*, L23808. doi: 10.1029/2006GL026731

Rex, M., Salawitch, R. J., von der Gathen, P., Harris, N. R. P., Chipperfield, M. P., & Naujokat, B. (2004). Arctic ozone loss and climate change. *Geophysical Research Letters*, *31*, L04116. doi: 10.1029/2003GL018844

Richter, A., Wittrock, F., Weber, M., Beirle, S., Kühl, S., Platt, U., … Burrows, J. P. (2005). GOME observations of stratospheric trace gas distributions during the splitting vortex event in the Antarctic winter of 2002. Part I: Measurements. *Journal of the Atmospheric Sciences*, *62*, 778–785. doi: 10.1175/JAS-3325.1

Rieder, H. E., & Polvani, L. M. (2013). Are recent Arctic ozone losses caused by increasing greenhouse gases? *Geophysical Research Letters*, *40*, 4437–4441. doi: 10.1002/grl.50835

Rozanov, V., Rozanov, A., Kokhanovsky, A., & Burrows, J. (2014). Radiative transfer through terrestrial atmosphere and ocean: Software package SCIATRAN. *Journal of Quantitative Spectroscopy and Radiative Transfer*, *133*, 13–71. doi: 10.1016/j.jqsrt.2013.07.004

Solomon, S. (1999). Stratospheric ozone depletion: A review of concepts and history. *Reviews of Geophysics*, *37*, 275–316. doi: 10.1029/1999RG900008

Solomon, S., Ivy, D. J., Kinnison, D., Mills, M. J., Neely, R. R., & Schmidt, A. (2016). Emergence of healing in the Antarctic ozone layer. *Science*, *353*, 269–274. doi: 10.1126/science.aae0061

Solomon, S., Kinnison, D., Bandoro, J., & Garcia, R. (2015). Simulation of polar ozone depletion: An update. *Journal of Geophysical Research: Atmospheres*, *120*, 7958–7974. doi: 10.1002/2015JD023365

Spang, R., Hoffmann, L., Müller, R., Grooß, J.-U., Tritscher, I., Höpfner, M., … Riese, M. (2018). A climatology of polar stratospheric cloud composition between 2002 and 2012 based on MIPAS/Envisat observations. *Atmospheric Chemistry and Physics*, *18*, 5089–5113. doi: 10.5194/acp-18-5089-2018

Strahan, S. E., Douglass, A. R., & Steenrod, S. D. (2016). Chemical and dynamical impacts of stratospheric sudden warmings on Arctic ozone variability. *Journal of Geophysical Research: Atmospheres*, *121*, 11,836–11,851. doi: 10.1002/2016JD025128

Tegtmeier, S., Rex, M., Wohltmann, I., & Krüger, K. (2008). Relative importance of dynamical and chemical contributions to Arctic wintertime ozone. *Geophysical Research Letters*, *35*, L17801. doi: 10.1029/2008GL034250

Veefkind, J. P., Aben, I., McMullan, K., Förster, H., de Vries, J., Otter, G., … Levelt, P. F. (2012). TROPOMI on the ESA Sentinel-5 Precursor: A GMES mission for global observations of the atmospheric composition for climate, air quality and ozone layer applications. *Remote Sensing of Environment*, *120*, 70–83. doi: 10.1016/j.rse.2011.09.027

Wagner, T., Leue, C., Pfeilsticker, K., & Platt, U. (2001). Monitoring of the stratospheric chlorine activation by Global Ozone Monitoring Experiment (GOME) OClO measurements in the austral and boreal winters 1995 through 1999. *Journal of Geophysical Research: Atmospheres*, *106*, 4971–4986. doi: 10.1029/2000JD900458

Weber, M., Coldewey-Egbers, M., Fioletov, V. E., Frith, S. M., Wild, J. D., Burrows, J. P., … Loyola, D. (2018). Total ozone trends from 1979 to 2016 derived from five merged observational datasets – the emergence into ozone recovery. *Atmospheric Chemistry and Physics*, *18*, 2097–2117. doi: 10.5194/acp-18-2097-2018

Weber, M., Dhomse, S., Wittrock, F., Richter, A., Sinnhuber, B.-M., & Burrows, J. P. (2003). Dynamical control of NH and SH winter/spring total ozone from GOME observations in 1995–2002. *Geophysical Research Letters*, *30*, 1583. doi: 10.1029/2002GL016799

Weber, M., Dikty, S., Burrows, J. P., Garny, H., Dameris, M., Kubin, A., ... Langematz, U. (2011). The Brewer-Dobson circulation and total ozone from seasonal to decadal time scales. *Atmospheric Chemistry and Physics*, *11*, 11221–11235. doi: 10.5194/acp-11-11221-2011

Weber, M., Eichmann, K.-U., Wittrock, F., Bramstedt, K., Hild, L., Richter, A., ... Müller, R. (2002). The cold Arctic winter 1995/96 as observed by GOME and HALOE: Tropospheric wave activity and chemical ozone loss. *Quarterly Journal of the Royal Meteorological Society*, *128*, 1293–1319. doi: 10.1256/003590002320373300

Wohltmann, I., Gathen, P., Lehmann, R., Maturilli, M., Deckelmann, H., Manney, G. L., ... Rex, M. (2020). Near-complete local reduction of Arctic stratospheric ozone by severe chemical loss in spring 2020. *Geophysical Research Letters*, *47*. doi: 10.1029/2020GL089547

Yulaeva, E., Holton, J. R., & Wallace, J. M. (1994). On the cause of the annual cycle in tropical lower-stratospheric temperatures. *Journal of the Atmospheric Sciences*, *51*, 169–174. doi: 10.1175/1520-0469(1994)051⟨0169:OTCOTA⟩2.0.CO;2